bution of improved alignment of individual molecules. The inverse dependence of the slower relaxation time scale on the shear rate suggests that the domains are being reduced in size by hydrodynamic forces.

Unfortunately, dichroism measurements made at a single wavelength cannot distinguish between changes in domain anisotropy and changes in their density. Domain multiplication and reduction have both been observed to occur as a result of flow,[19] and any coupling of these two possibilities cannot be unambiguously interpreted with this measurement. Since conservative dichroism can be expected to be a strong function of the ratio of the size of the scattering structures to the wavelength, scanning wavelength would offer the possibility of directly determining the population densities of domains according to their size. Such an experiment would be valuable in understanding the reasons why the transmitted light intensity decreased with flow rate of the more highly concentrated, racemic mixture.

Although many features of the dichroism and shear stress measurements were similar, a few noticeable differences were observed. In particular, reproducible results could often be obtained in the mechanical measurements during conditions where the measurement of dichroism resulted in irreproducible and often chaotic signals. This occurred during relaxation following flow cessation and during flow as the shear rates approached values where the first normal shear difference crossed from positive to negative values. The most probable explanation for these differences is that the stress measurements are averages over the entire surfaces of a force transducer whereas the dichroism measurement is made over a localized volume element. This would cause possible spatial variations to be averaged in the mechanical measurements, which would minimize or eliminate the temporal variations which might result.

An additional point of difference between the optical and mechanical measurements was that, whereas flow reversal and step changes in shear rate produced similar mechanical effects, the same was not true for the optical measurements. This is related to the fact that the dichroism is a rather weak, decreasing function of shear rate while the shear stress is a strong, increasing function of this parameter. For that reason, a step change in shear rate would not be expected to result in a large transient. A flow reversal, on the other hand, produces a dramatic restructuring of the fluid and leads to large effects in both the mechanical and optical measurements.

Acknowledgment. The dichroism measurements were motivated by preliminary measurements performed by P. L. Frattini and C. Cathey while graduate students at Stanford University. We are grateful to J. Starita for facilitating this collaboration. Funding of the optical measurements was through the Presidential Young Investigator Grant CBT 84-51446 from the National Science Foundation to G.F. The samples have been generously donated by Celanese Research through Dr. K. Wissburn.

Registry No. PBLG (homopolymer), 25014-27-1; PBLG (SRU), 25038-53-3; PBDG (homopolymer), 30869-19-3; PBDG (SRU), 31724-32-0.

References and Notes

(1) Wissbrun, K. F. *J. Rheol.* **1981**, 25, 619.
(2) Asada, T.; Onogi, S.; Yanase, H. *Polym. Eng. Sci.* **1984**, *24*, 355.
(3) Kiss, G.; Porter, R. S. *J. Polym. Sci., Polym. Symp.* **1978**, *65*, 193.
(4) Kiss, G.; Porter, R. S. *J. Polym. Sci., Polym. Phys. Ed.* **1980**, *18*, 361.
(5) Moldenaers, P.; Mewis J. *J. Rheol.* **1986**, *30*, 567.
(6) Navard, P. *J. Polym. Sci., Polym. Phys. Ed.* **1986**, *24*, 435.
(7) Moldenaers, P.; Mewis, J. *World Congress Chem. Eng., III* **1986**, *4*, 546.
(8) Mewis, J.; Moldenaers, P. *Mol. Cryst. Liq. Cryst.* **1987**, *153*, 291.
(9) Viola, G. G.; Baird, D. G. *J. Rheol.* **1986**, *30*, 601.
(10) Wood, B. A.; Thomas, E. L. *Nature (London)* **1986**, *324*, 655.
(11) Marrucci, G. *Rheol.*, [*Proc. Int. Congr.*], *9th* **1984**, *1*, 441.
(12) Brinkman, W. F.; Cladis, P. E. *Phys. Today* **1982**, *35*, 48.
(13) Wissbrun, K. F. *Faraday Discuss. Chem. Soc.* **1985**, *79*, 161.
(14) Moldenaers, P.; Mewis, J. *Chem. Eng. Commun. 53*, **1987**, 33.
(15) Frattini, P. L.; Fuller, G. G. *J. Fluid Mech.* **1986**, *168*, 119.
(16) Moldenaers, P.; Mewis, J. *Die Macromol. Chem.*, to be published.
(17) Marrucci, G.; Grizzuti, N. Constitutive Equations for Liquid Crystalline Polymers; paper presented at the 59th Annual Meeting of the Society of Rheology, Atlanta, GA, October 18–22, 1987.
(18) de Gennes, P.-G. *The Physics of Liquid Crystals*; Clarendon: Oxford, 1974.
(19) Alderman, N. J.; Mackley, M. R. *Faraday Discuss. Chem. Soc.* **1985**, *79*, paper 12.

Self-Consistent Field Theory of Surfaces with Terminally Attached Chains

M. Muthukumar*

Polymer Science and Engineering Department, University of Massachusetts, Amherst, Massachusetts 01003

Jyh-Shyong Ho

Chemistry Department, University of Massachusetts, Amherst, Massachusetts 01003.
Received February 25, 1988; Revised Manuscript Received July 9, 1988

ABSTRACT: Considering a planar surface with many terminally attached polymer chains at a distance d to another planar surface, we have solved numerically the differential equation for the probability distribution function of an effective chain within the self-consistent field approximation. We have calculated (a) segmental density profiles of the chains and (b) free energy of interaction vs d profiles for both repulsive and attractive two-body excluded volume interaction and for both adsorbing and nonadsorbing surfaces. The contributions from the osmotic and bridging effects to the free energy–d profiles are systematically calculated, and the results are compared with experiments on forces between surfaces bearing polystyrene in near-Θ solutions and with block copolymers.

1. Introduction

The configurations of terminally attached polymer chains at an interface have attracted considerable interest[1] both experimentally and theoretically in view of their role in colloidal stability, copolymer morphology, adhesives, etc. The chain configurations in the proximity of surfaces are

0024-9297/89/2222-0965$01.50/0

altered significantly when the solvent quality, nature of polymer–surface interaction, etc., are changed. These modifications in the chain configurations manifest in the experimentally observed differences in behaviors such as segment density distributions and force–separation profiles under different conditions. In this paper we present results of numerical calculations of free energy of two surfaces of terminally attached chains as a function of solvent quality and the strength of polymer–surface attraction.

Previous theoretical treatments[2-17] of polymer attached surfaces have employed lattice models, scaling arguments, and self-consistent field (SCF) methods. Among these approaches, the SCF method appears to be in better agreement with experimental data. The SCF method has been extensively used to treat terminally attached chains[4,5,14,15,17] and other similarly constrained polymers such as block copolymers.[18,19] This method was introduced[5] first by Dolan and Edwards to study the effect of excluded volume on the free energy of two plane surfaces of terminally grafted chains. However, they studied only nonadsorbing surfaces and repulsive monomer interactions (i.e., temperatures above Θ temperature). Some limiting cases of the Dolan–Edwards study can be handled analytically.[20-22]

Among the various experimental techniques[23] used to study the behavior of adsorbed polymer layers, the direct measurement[24-32] of the force as a function of distance between two polymer-containing surfaces has been of considerable interest. From the direct measurement of force–separation profiles between adsorbed layers of polystyrene on mica immersed in cyclohexane, Klein[26,27] observed that the profiles show an attractive minimum at temperatures (T) below the Θ temperature Θ at which the bulk second virial coefficient vanishes. Klein also conjectured that the attraction originates from the entry, with decreasing separation, into the two-phase unstable region of the bulk polystyrene–cyclohexane phase diagram. It was later shown by Israelachvili et al.[28] that attractive force is present for this system even at temperatures above Θ. These authors suggested that the simultaneous adsorption of a single chain to both surfaces, called "bridging", could be responsible for the observed attractive force–separation profile. The recent work of Hadziioannou et al.[31] on adsorbed layers of block copolymers, where bridging is essentially eliminated, shows that the force–separation profile is attractive if $T < \Theta$ but repulsive if $T \geq \Theta$.

It is therefore desirable to perform a theoretical calculation for terminally attached chains for different values of the second virial coefficient (both positive ($T > \Theta$) and negative ($T < \Theta$)) and different strengths of attractive interaction between the surface and the polymer segments. In this paper we apply the method of Dolan and Edwards[5] to calculate the free energy–separation profile for both repulsive and attractive effective excluded volume between polymer segments and both unadsorbing and adsorbing surfaces. In these calculations the two-body segment interactions are replaced by a position-dependent segment chemical potential arising self-consistently from the calculated segment density profile. We calculate systematically the contributions of osmotic and adsorption effects to the segment density and free energy–separation profiles.

The model is described in section II, the calculational procedure is given in section III, and the results are discussed in section IV.

2. Model

We consider a collection of N polymer chains which are uniformly end-grafted to a planar surface of area A. This surface appears like a "brush" containing N floppy (or soft) bristles. The monomers of the chains undergo the excluded volume interaction among themselves and attractive interaction with the surface. Furthermore, these chains are confined by another planar surface of area A which is parallel to the first surface at a distance d (see parts a and b of Figure 1). In type a, the second surface is a hard wall and does not contain any chemically anchored chains. Since the second surface is a hard wall it cannot adsorb the chains. It is used only to confine the chains anchored to the first surface which can adsorb the chains. Here the bridging of chains between two surfaces is forbidden. In type b, the second surface also contains N end-grafted chains, and the $2N$ chains are confined by the surfaces which can in principle adsorb the chains.

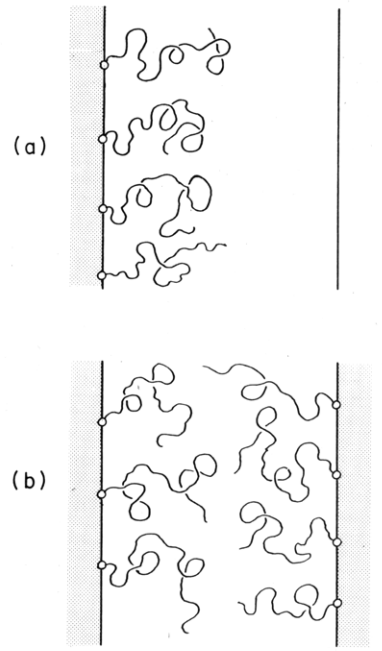

Figure 1. Schematic representation of two cases studied here. In type a, one surface contains terminally attached chains and the other surface is a hard wall. In type b, both surfaces contain terminally attached chains.

Let L be the chain length for each of the chains. If the polymer chains are represented as continuous curves, the total probability distribution function $\mathcal{P}$ for all the chains is given by the Edwards path integral

$$\mathcal{P} = \int \mathrm{d}[\mathbf{r}_i(s)] \exp\left[-\frac{3}{2l} \sum_{i=1}^{N} \int_0^L \mathrm{d}s_i \left(\frac{\partial \mathbf{r}_i(s_i)}{\partial s_i} \right)^2 - \sum_{i,j=1}^{N} \int_0^L \mathrm{d}s_i \int_0^L \mathrm{d}s_j \, W[\mathbf{r}_i(s_i) - \mathbf{r}_j(s_j)] - \beta \sum_{i=1}^{N} \int_0^L \mathrm{d}s_i \, V[\mathbf{r}_i(s_i)] \right] \quad (2.1)$$

where $\mathbf{r}_i(s_i)$ is the position vector of the arc length variable s_i ($0 \leq s_i \leq L$) of the ith chain. l is the Kuhn step length. $W[\mathbf{r}_i(s_i) - \mathbf{r}_j(s_j)]$ is the effective pairwise interaction energy between the s_i and s_j monomers at $\mathbf{r}_i(s_i)$ and $\mathbf{r}_j(s_j)$. $V[\mathbf{r}_j(s_j)]$ is the total interaction energy between the jth monomer and the surfaces. $\beta = 1/k_B T$ with k_B the Boltzmann constant and T the absolute temperature. The symbol $\int \mathrm{d}[\mathbf{r}_j(s)]$ denotes functional integration representing the sum over all possible chain configurations. The conditional probability distributions, such as the probability distribution function $G_i(\mathbf{R},\mathbf{R}';L,0)$ for the ith chain to have its ends at $\mathbf{R}$ and $\mathbf{R}'$, are obtained by imposing these constraints as the appropriate limits of the path integrals:

$$\int_{\mathbf{r}_i(0)=\mathbf{R}'}^{\mathbf{r}_i(L)=\mathbf{R}} \mathrm{d}[\mathbf{r}_i(s)]$$

We take the effective pairwise interaction energy W to be a point contact pseudopotential[33] of strength v

$$W[\mathbf{r}_i(s_i) - \mathbf{r}_j(s_j)] = \frac{v}{l^2}\delta[\mathbf{r}_i(s_i) - \mathbf{r}_j(s_j)] \tag{2.2}$$

where δ is the Dirac δ function. The excluded volume parameter v can be interpreted as the angular averaged binary cluster integral for a pair of segments in the discrete chain model

$$v \equiv \frac{1}{2}\left\langle \int \mathrm{d}\mathbf{r}_{ij}[1 - e^{-\beta u(\mathbf{r}_{ij})}]\right\rangle \tag{2.3}$$

where $u(\mathbf{r}_{ij})$ is the pair potential of mean force between the ith and jth segments as a function of separation $\mathbf{r}_{ij}$.

We assume that the potential interaction energy between the sth segment and a surface element of area d^2S is given by the van der Waals attractive energy

$$\beta V(\mathbf{r}(s)) = \epsilon'(l/r)^6 \tag{2.4}$$

where r is the distance of $\mathbf{r}(s)$ from the center of the surface element.

The integral equation (2.1) can be exactly replaced by the differential equation for each chain

$$\left[\frac{\partial}{\partial s} - \frac{l}{6}\nabla_{\mathbf{r}}^2 + \sum_{j=1}^{N}\int_0^L \mathrm{d}s_j\, W(\mathbf{r} - \mathbf{r}(s_j'')) + \beta V(\mathbf{r})\right] G_i(\mathbf{r},\mathbf{r}';s,s') = \delta(\mathbf{r} - \mathbf{r}')\delta(s - s') \tag{2.5}$$

with the boundary condition that the Green function G_i vanishes if $\mathbf{r}$ approaches infinity or any surface in the system. The subscript i of s is dropped for notational convenience. Even when the surface potential V is absent, eq 2.5 is impossible to solve exactly. We employ the same self-consistent field method developed by Edwards[3-5] to study the excluded volume effect. Although this method is not adequate in the dilute limit where there are substantial monomer density fluctuations, the self-consistent field method becomes satisfactory in the higher density situations corresponding to sufficiently high surface density of polymers studied here.

By generalizing Edwards' method to the presence of the extra βV term, we obtain the self-consistent equation for $G_i(\mathbf{r},\mathbf{r}';s,s')$:

$$\left[\frac{\partial}{\partial s} - \frac{l}{6}\nabla_{\mathbf{r}}^2 + \frac{v}{l^2}\tilde{p}(\mathbf{r}) + \beta V(\mathbf{r})\right] G_i(\mathbf{r},\mathbf{r}';s,s') = \delta(\mathbf{r} - \mathbf{r}')\delta(s - s') \tag{2.6}$$

$$\frac{1}{l}\tilde{p}(\mathbf{r}) = \frac{1}{l}\sum_{i=1}^{N}\tilde{p}_i(\mathbf{r}) \tag{2.7}$$

where $\tilde{p}(\mathbf{r})/l$ is the total segment density, with $\tilde{p}_i(\mathbf{r})$ for the ith chain with its end ($s \to 0$) at $\mathbf{R}_i'$ given by

$$\frac{1}{l}\tilde{p}_i(\mathbf{r}) = \frac{\int_0^L \mathrm{d}s\; G_i(\mathbf{r},\mathbf{R}_i';s,0)\int \mathrm{d}\mathbf{r}''\; G_i(\mathbf{r}'',\mathbf{r};L,s)}{\int \mathrm{d}\mathbf{r}''\; G_i(\mathbf{r}'',\mathbf{R}_i';L,0)} \tag{2.8}$$

If the surface coverage is uniform and so large that the probability of finding a segment s from any of the chains at $\mathbf{r}$ is a function of the perpendicular distance x of $\mathbf{r}$ from the surface, then $\tilde{p}(\mathbf{r})$ is a function of x only. After integration over the two directions parallel to the surfaces, eq 2.6 for an effective chain becomes[5]

$$\left[\frac{\partial}{\partial s} - \frac{l}{2}\frac{\partial^2}{\partial x^2} + \frac{v}{l^2}\tilde{p}(x) + \beta\tilde{V}(x)\right] G(x,x';s) = \delta(x - x')\delta(s - s') \tag{2.9}$$

where

$$\tilde{p}(x) = \frac{N}{A}\frac{\int_0^L \mathrm{d}s\; G(x,0;s)\int \mathrm{d}x''\; G(x'',x;L-s)}{\int \mathrm{d}x''\; G(x'',0;L)} \tag{2.10}$$

$$\tilde{p}(x) \equiv \frac{N}{A}\hat{p}(x) \tag{2.11}$$

and $\beta\tilde{V}(x)$ is the truncated and integrated van der Waals attractive potential energy between a segment and a surface

$$\beta\tilde{V}(x) = -\frac{\epsilon}{l}\left(\frac{l}{x}\right)^3; \quad l \leq x \leq d - l \tag{2.12}$$

with ϵ the Hamaker constant.[1] In eq 2.10, the constraint of end-grafting of the chains is explicitly expressed.

In the absence of the surfaces, the dimensionless excluded volume parameter[5] for the one-dimensional case considered here is $vL^{3/2}l^{-9/2}$. Since the excluded volume effect of all chains is taken as the sum of contributions from individual chains in a self-consistent field, the dimensionless excluded volume parameter[5] turns out to be

$$u \equiv \frac{NvL^{3/2}}{Al^{5/2}} \tag{2.13}$$

We solve the one-dimensional equation (2.9) numerically for different values of u and ϵ/l using a self-consistent procedure and the boundary condition that $G(x,0;s)$ is zero if s is on any surface.

3. Calculations

We solve eq 2.9 numerically by discretizing the (s,x) space into a rectangular grid with the Kuhn length l being the grid spacing in both the s and x directions. Thus

$$\begin{aligned} s &= (i-1)l; \quad i = 1, \ldots, n+1 \\ x &= (j-1)l; \quad j = 1, \ldots, m+1 \\ x' &= (k-1)l; \quad k = 1, \ldots, m+1 \end{aligned} \tag{3.1}$$

where $n = L/l$ and $m = d/l$. For the chain end-grafted to the surface, one end ($s = 0$, i.e., $i = 1$) is at the surface ($k = 1$). Since this is difficult to handle in the discrete space, we assume that the chain starts at some position very close to the surface, and the calculation is carried out for all $i > 1$. In other words, we ignore the first monomer. Furthermore, the right-hand side of eq 2.9 is zero since $\delta(s) = 0$ for $s \neq 0$.

The various factors of eq 2.9 in the discretized space become

$$\begin{aligned} \frac{\partial}{\partial s}G(x,x';s) &\to \frac{1}{l}[G(j,k;i+1) - G(j,k;i)] \\ \frac{\partial^2}{\partial x^2}G(x,x';s) &\to \frac{1}{l^2}[G(j+1,k;i) + G(j-1,k;i) - 2G(j,k;i)] \\ G(x,x';s) &\to \frac{1}{2}[G(j+1,k;i) + G(j-1,k;i)] \end{aligned} \tag{3.2}$$

Therefore, eq 2.9–2.12 can be rewritten as

$$G(j,k;i+1) = \frac{1}{2}[G(j+1,k;i) + G(j-1,k;i)]\left[1 - \frac{vN}{Al}\frac{\hat{p}(j)}{l} - \beta\tilde{V}(j)\right] \tag{3.3}$$

where

$$\frac{\hat{p}(j)}{l} = \frac{\sum_{i=2}^{n}\sum_{k'=1}^{m+1} G(j,2;i)\, G(k',j;n+2-i)}{\sum_{k'=1}^{m+1} G(k',2;n+1)} \quad (3.4)$$

and

$$\beta\tilde{V}(j) = -\frac{\epsilon}{l}(j-1)^{-3}; \quad j = 2, ..., m \quad (3.5)$$

It must be noted that for type b (see Figure 1b), where both surfaces contain end-grafted polymer chains, $\hat{p}(j)$ must be replaced by

$$\hat{p}(j) \rightarrow \frac{1}{2}[\hat{p}(j) + \hat{p}(m-j)]; \quad j = 2, ..., m \quad (3.6)$$

In addition, for type b, $\beta V(j)$ should have an additional term, $-(\epsilon/l)(m+1-j)^{-3}$ (with $2 < j < m$), due to the second surface. Equation 3.3 is solved by using an iterative procedure. By using an approximation to G, we obtained $\hat{p}$ from eq 3.4, from which a further approximation for G is calculated from eq 3.3. The process is repeated until the self-consistent solution for G is reached. We have used the exact solution $G^{(0)}$ of eq 2.9 with v and $\beta\tilde{V}$ absent as the initial trial for G in the iterative procedure. $G^{(0)}$ is given by

$$G^{(0)}(x,x';s) = \frac{2}{d}\sum_{p=1}^{\infty}\sin\left(\frac{\pi p x}{d}\right)\sin\left(\frac{\pi p x'}{d}\right)\exp\left(-\frac{\pi^2 p^2 l s}{2d^2}\right) \quad (3.7)$$

which becomes in the discretized notation

$$G^{(0)}(j,k;i) = \frac{2}{ml}\sum_{p=1}^{M}\sin\left(\frac{\pi p(j-1)}{m}\right)\sin\left(\frac{\pi p(k-1)}{m}\right)\times \exp\left(-\frac{\pi^2 p^2 (i-1)}{2m^2}\right) \quad (3.8)$$

Here M is a sufficiently large number (typically $M = 80$ in our calculations).

Thus, the methodology for the iteration procedure is as follows for a given set of values of the parameters $(v, \beta\tilde{V})$. (1) Calculate $\hat{p}^{(0)}(j)$ for all $j = 1, ..., m+1$ by using $G^{(0)}(j,k;i)$. (2) Substitute $\hat{p}^{(0)}(j)$ and $G^{(0)}(j,k;i)$ into the right-hand side of eq 3.3 and calculate $G^{(1)}(j,k;i)$ for all possible values of j, k, and i. (3) Calculate $\hat{p}^{(1)}(j)$ for all j by using $G^{(1)}(j,k;i)$. (4) Compare $|\hat{p}^{(1)}(j) - \hat{p}^{(0)}(j)|$ with λ ($\sim 1.0 \times 10^{-6}$). If $|\hat{p}^{(1)}(j) - \hat{p}^{(0)}(j)| < \lambda$, the calculation is completed. Otherwise, repeat steps 2 and 3 to get $G^{(2)}$ and $\hat{p}^{(2)}$ and go to step 4 as many number $(\alpha - 1)$ of times as necessary to satisfy $|\hat{p}^{(\alpha)}(j) - \hat{p}^{(\alpha-1)}(j)| \leq \lambda$ for all i. (5) Use $G^{(\alpha)}$ to calculate all the necessary quantities of physical interest such as the monomer density profiles and the free energy of separation between the surfaces at d.

4. Results and Discussion

a. Density Profiles. The segment density profile, $\hat{p}(x)/l$, has been calculated numerically from eq 2.9 and 2.10 for both types a and b. We have chosen $n = 400$, and the calculations were performed for $u = -5$, 0, 5, and 10, $\epsilon/l = 0$, 0.25, 0.5, 1.0, 1.25, and 2.5, and $d/l = 10$, 20, 40, and 80. The results for the first and second types are presented in Figures 2 and 3 and Figures 4 and 5, respectively. For the case of unadsorbing surfaces with a random flight chain ($u = 0 = \epsilon$), analytical expressions are available[4] for the density profiles, and the results are included in these figures for comparison.

The results for the case of $d/l = 20$ for different values of u and ϵ/l are presented in Figure 2a–c. In Figure 2a,

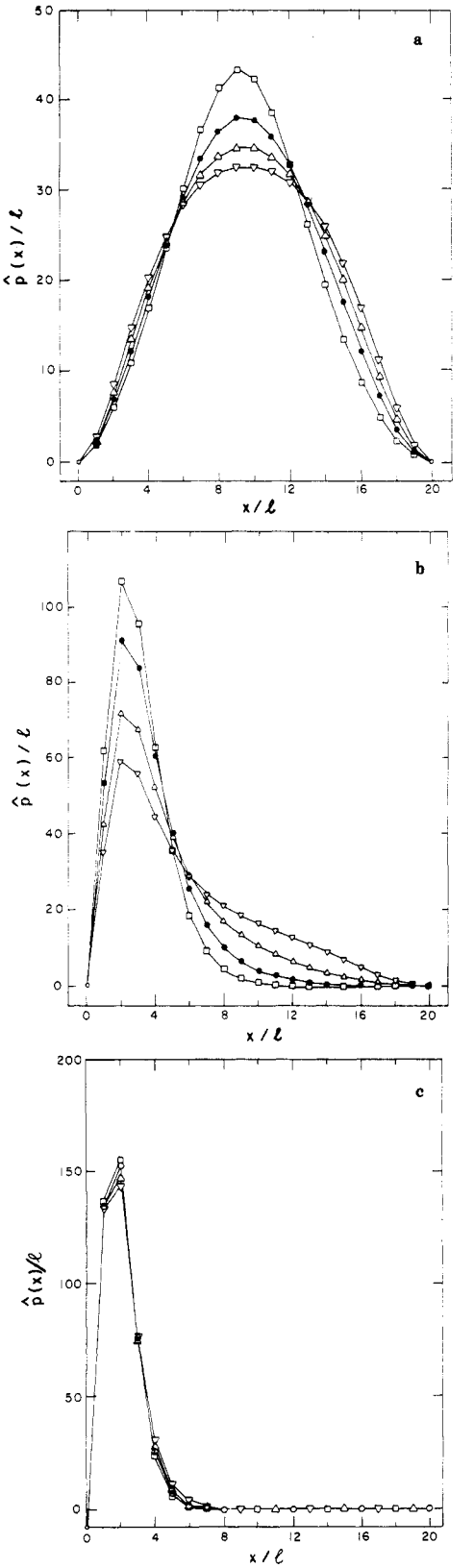

Figure 2. Plot of segment density profile, $\hat{p}(x)/l$, for type a vs x for $d/l = 20$ and different values of u and ϵ/l. The symbols □, ○, △, and ▽ correspond respectively to $u = -5$, 0, 5, and 10. Parts a–c correspond respectively to $\epsilon/l = 0$, 1.0, and 2.5.

where the adsorption energy ϵ is zero, the excluded volume effect broadens the density profiles. On the other hand, if the solution condition is below Θ state, e.g., $u = -5$, the segment density profile sharpens. When the attractive interaction energy between the surface and the polymer becomes progressively stronger (see Figure 2a–c), the

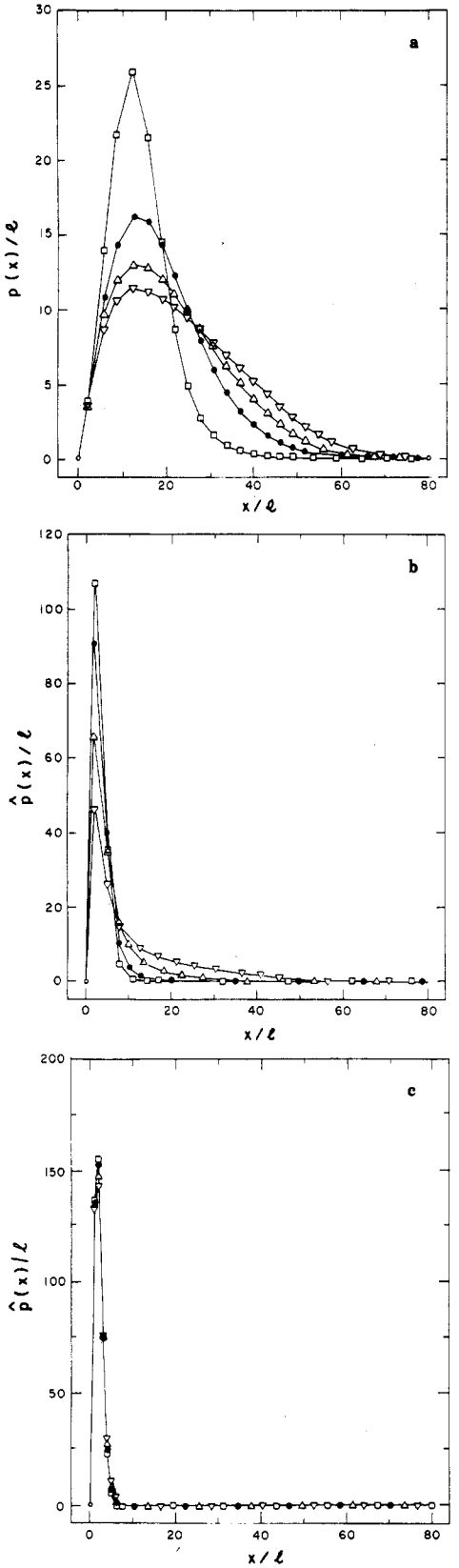

Figure 3. Plot of segment density profile, $\hat{p}(x)/l$, for type a vs x for $d/l = 80$ and different values of u and ϵ/l. The symbols have the same meaning as in Figure 2.

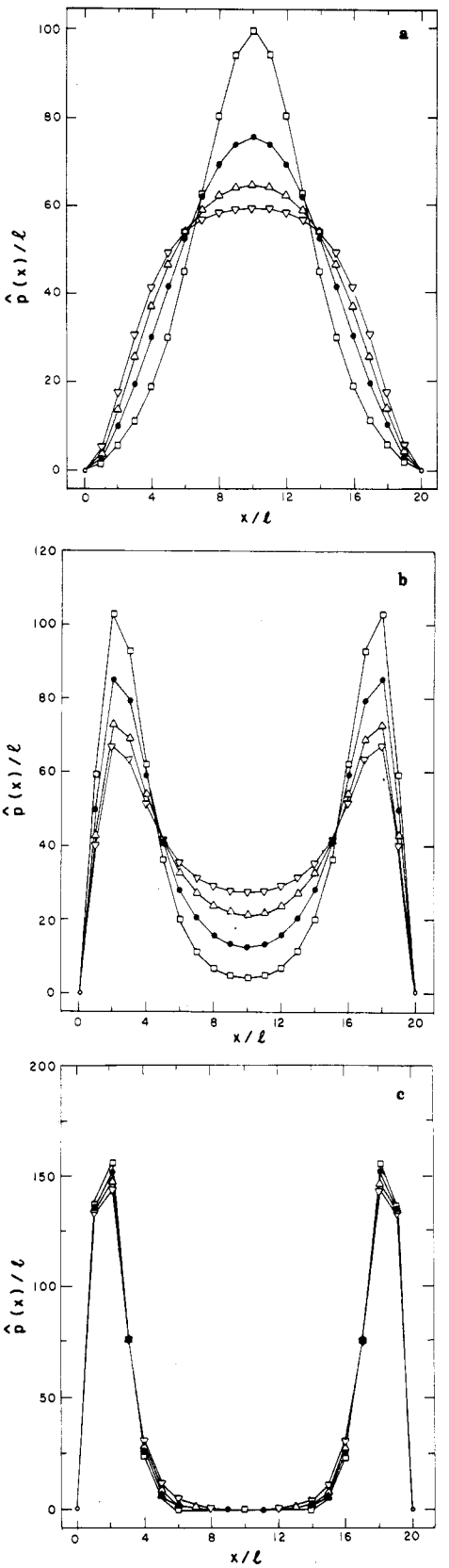

Figure 4. Plot of segment density profile, $\hat{p}(x)/l$, for type b vs x for $d/l = 20$ and different values of u and ϵ/l. The symbols have the same meaning as in Figure 2.

position of the maximum of the density profile moves toward the surface for all values of u. For sufficiently large values of ϵ/l, the observed density profile is independent of the values of u studied here.

The numerical results of $\hat{p}(x)$ for $d/l = 80$ are given respectively in Figure 3. Similar profiles are obtained for intermediate separations. The same trends as in the series of Figure 2 are observed in Figure 3 also. The density profiles are broader as the surfaces are moved further apart since the polymer segments have more freedom due to less confinement.

When both surfaces contain grafted polymer chains, the density profiles are given in Figures 4 and 5 corresponding

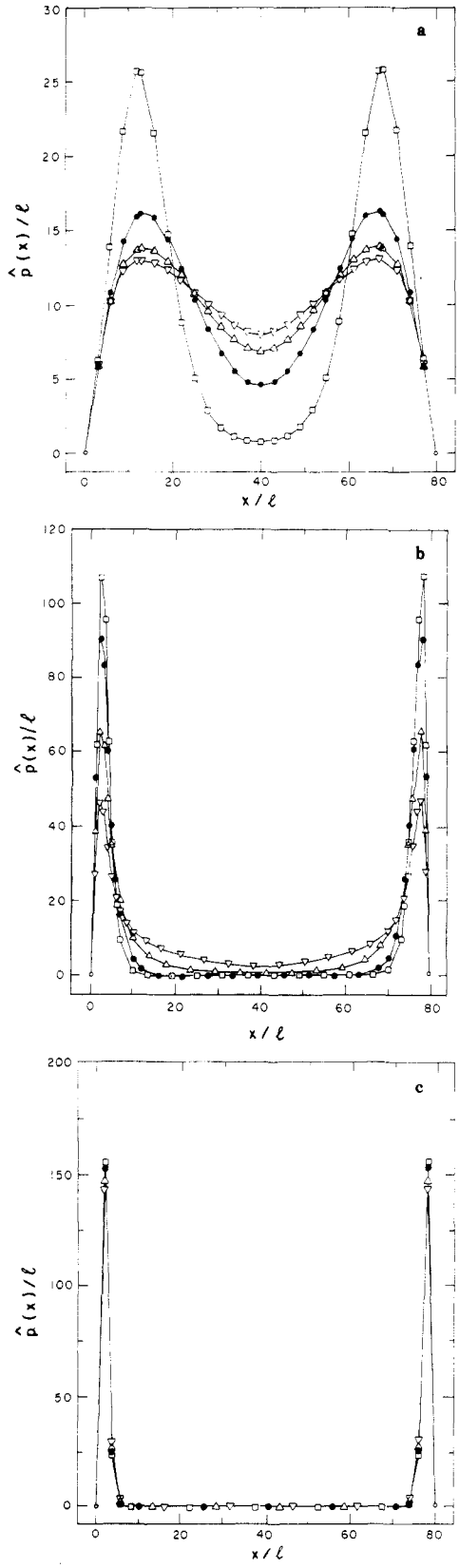

Figure 5. Plot of segment density profile for type b vs x for d/l = 80 and different values of u and ϵ/l. The symbols have the same meaning as in Figure 2.

respectively to d/l = 20 and 80. It is clear from Figure 4a that the presence of excluded volume effect flattens the density profiles. On the other hand, when the effective two-body interactions become attractive (u = −5), the density profile is sharp. All the profiles become broader as the strength of the attractive interaction between the

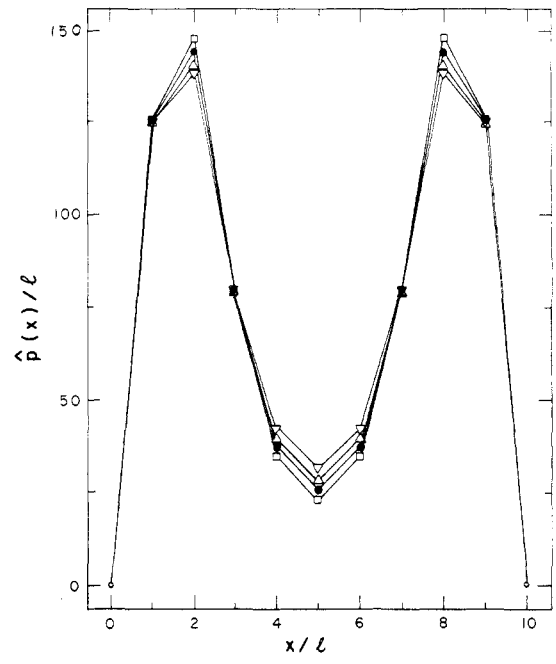

Figure 6. Plot of segment density profile for type b vs x for d/l = 10 and ϵ/l = 2.5. The symbols have the same meaning as in Figure 2.

polymer and the surfaces is increased (Figure 4a–c). However, for sufficiently large ϵ/l, the chains adsorb to the surfaces showing two peaks in the density profiles. The critical value of ϵ/l necessary for the dominant adsorption to the surface depends on the nature of the polymer solution. For example, the density profile for u = 10 shows a double maximum near the surfaces when ϵ/l = 0.5 while the profile for u = −5 shows a density buildup in the bulk. On the other hand, when ϵ/l = 1.0, even the case of u = −5 exhibits two peaks in the density profile. This feature is in agreement with the recent Monte Carlo simulations.[35]

The dependencies of the density profiles on u and ϵ depend also on the separation between the surfaces, as shown in Figures 4 and 5. The trends are similar to those observed in type a. If the surfaces are close enough and if the adsorption is sufficiently strong, then bridging is prevalent. This is illustrated in Figure 6, where segment density profile is presented for ϵ/l = 2.5 and d/l = 10. These profiles are to be compared with those of Figures 4c and 5c. In Figure 6, the heights of the peaks near the surfaces are smaller and the density in the middle is higher. On the other the other hand, for large separations (as in Figures 4c and 5c), the chain adsorbs to one surface only with diminished bridging.

Our calculated results are in complete agreement with those of Dolan and Edwards,[5] where u = 0, 5, and 10 was considered at ϵ = 0. By replotting the results of Figures 2–5 as double logarithmic graphs of the segment density versus x, we have attempted to obtain the scaling exponents predicted by Alexander[7] and de Gennes.[6,10] However, our numerical results do not conform to any particular power law over any sufficiently long interval of x, as was also observed in the recent neutron-scattering studies[36] from adsorbed polymer layers.

b. Free Energy of Separation. The number of configurations, $\Omega(d)$, of the grafted polymer chains relative to the number of configurations of unconfined chains is given by

$$\Omega(d) = \int_0^d dx\ G(x,0;L) \tag{4.1}$$

where d is the separation distance of the plane surfaces

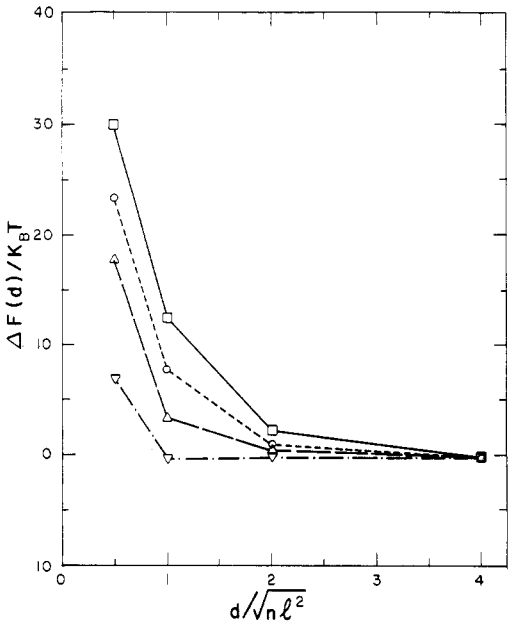

Figure 7. Plot of free energy profile $\Delta F(d)$ for type a vs $d/n^{1/2}l$ for $\epsilon = 0$ and different values of u (□, $u = 10$; ○, $u = 5$; △, $u = 0$; ▽, $u = -5$).

and G is calculated by using the procedure described above for different values of d. The free energy of separation, $\Delta F(d)$, relative to when the plane surfaces are separated by a large distance, d_∞, is obtained from

$$\Delta F(d) = \ln\left(\frac{\Omega(d)}{\Omega(d_\infty)}\right) \tag{4.2}$$

where $\Delta F(d)$ is calculated in units of k_BT. Although d_∞ should be infinite in the calculation of the reference state, we have taken $d_\infty/l = 80$ since the probability distribution for the end-to-end distance of the chain vanishes for such large separations. Furthermore, we have used the same reference state of $d_\infty/l = 80$ with polymer chains grafted to one surface only and the other surface free and unadsorbing in the calculation of $\Delta F(d)$ for both types a and b.

The numerical results of $\Delta F(d)$ for type a are plotted in Figures 7 and 8 versus $d/n^{1/2}l$ for different values of u and ϵ/l. Since one surface in type a is only a hard wall, bridging of the chain is not allowed in this situation. When the surface is unadsorbing ($\epsilon = 0$) (see Figure 7), the free energy of interaction is purely repulsive and is long-ranged even if the monomer interactions are attractive. The repulsive forces are present at separations equal to approximately 5 times the radius of gyration of a free random flight chain. The range of the repulsive interaction is substantially reduced as the strength of the excluded volume parameter is decreased from a good solvent ($u > 0$) to a poor solvent ($u < 0$). The onset of repulsion is much steeper in a poor solvent.

The influence of the presence of an attractive potential between the surface and the polymer chains is presented in parts a and b of Figure 8. If $u \geq 0$ (i.e., the temperature is Θ or above), the effect of the attractive surface potential is to reduce the range and the steepness of the $\Delta F(d)$ profiles. On the other hand, if the temperature is below Θ ($u < 0$), the adsorption potential near the surface results in a shallow free energy minimum. The depth of the free energy minimum increases with an increase in ϵ. The results of Figure 8b show that an attractive minimum should be observed at about 3 times the radius of gyration of a random flight chain in the force–separation profile. For very large ϵ, the monomers stick to the surface and the range of the interaction is very short.

Thus the origin of the attractive minimum in the force–separation profiles in type a is the attractive interaction between the polymer and the surface. The attractive minimum in $\Delta F(d)$ is observable independent of the quality of the solvent. The double logarithmic plots of the repulsive part of $\Delta F(d)$ profiles show that $\Delta F(d)$ does not decay with d strictly as a power law ($d^{-\alpha}$); nevertheless, a crude apparent value of 2.5 can be estimated for α.

The results of $\Delta F(d)$ for type b are plotted in Figures 9 and 10 versus $d/n^{1/2}l$ for different values of u and ϵ/l. In this situation both surfaces contain the grafted polymer chains and are capable of adsorbing the chains depending on the value of ϵ/l. When $\epsilon = 0$ so that bridging of a chain between two surfaces is not allowed, we see from Figure

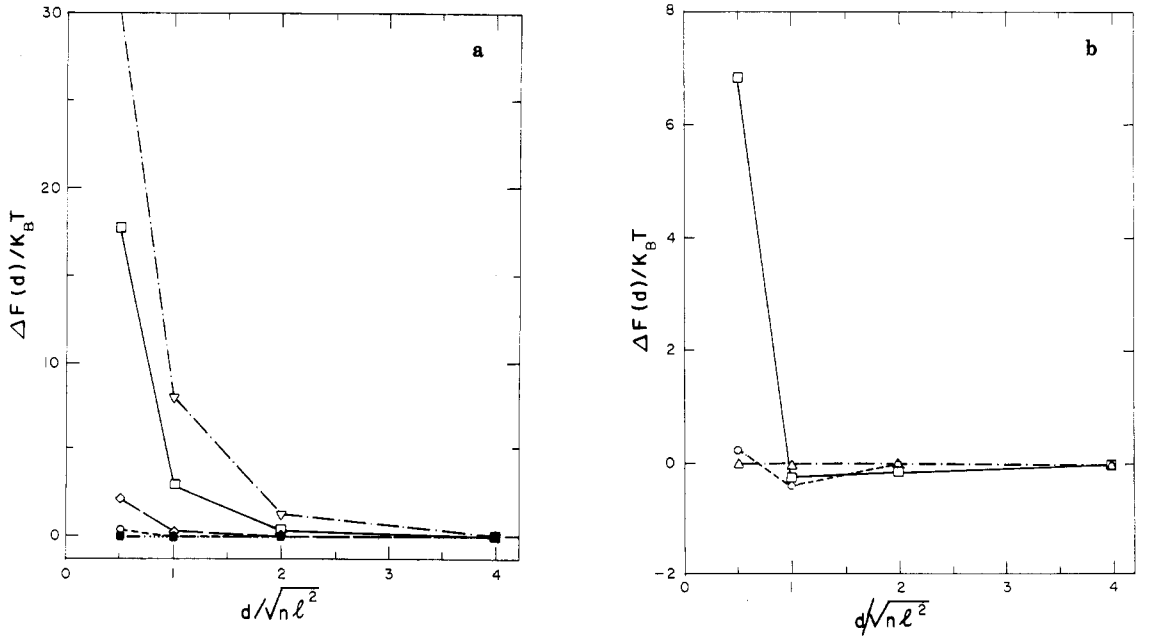

Figure 8. Plot of $\Delta F(d)$ for type a vs $d/n^{1/2}l$. In part a, the symbols □, ○, and △ correspond to $\epsilon/l = 0$, 1.25, and 2.5, respectively, for $u = 0$; ▽, ◇, and ■ correspond to $\epsilon/l = 0$, 1.25, and 2.5, respectively, for $u = 10$. In part b, $u = -5$ and the symbols □, ○, and △ correspond to $\epsilon/l = 0$, 1.25, and 2.5, respectively.

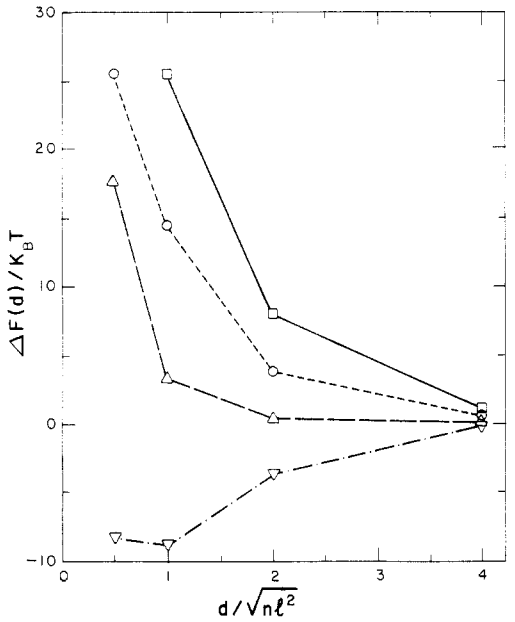

Figure 9. Plot of $\Delta F(d)$ for type b vs $d/n^{1/2}l$ for $\epsilon = 0$. The symbols are the same as in Figure 7.

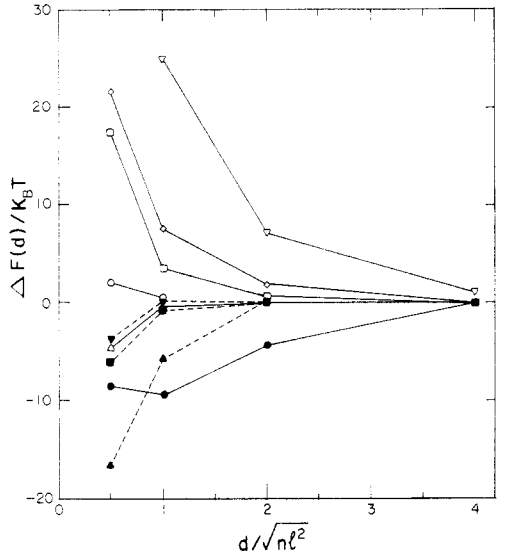

Figure 10. Plot of $\Delta F(d)$ for type b vs $d/n^{1/2}l$ for different values of u and ϵ. The symbols □, ○, and △ correspond to $\epsilon/l = 0$, 0.5, and 2.5, respectively, for $u = 0$; ▽, ◇, and ■ correspond to $\epsilon/l = 0$, 1.0, and 2.5, respectively, for $u = 10$; ●, ▲, and ▼ correspond to $\epsilon/l = 0$, 0.5, and 2.5, respectively, for $u = -5$.

9 that $\Delta F(d)$ profiles are purely repulsive for $u \geq 0$ but show an attractive minimum for $u = -5$. These features are in excellent agreement with the experimental observations.[31,32] This attractive minimum is due to the buildup of the segment density near the surface (see Figures 4–6), and the segments themselves undergo attractive interaction ($u < 0$). From the discretized $\Delta F(d)$ profile for $u = -5$ and $\epsilon = 0$ we expect an attractive minimum in the force–separation profile at about 3 times the radius of gyration of a random flight configuration.

When $\epsilon > 0$, so that bridging of the chain is possible (see also Figure 6), $\Delta F(d)$ can become attractive. The magnitude of the attractive free energy and the range of attraction of $\Delta F(d)$ profiles depend on the values of u and ϵ. At the Θ temperature ($u = 0$), ΔF shows an attractive minimum if $\epsilon/l \geq 1.0$ (Figure 10). If u is increased from 0 to 5 and 10, then $\Delta F(d/n^{1/2}l = 0.5)$ for $\epsilon/l = 1.25$ changes from −8.2 to −3.0 and 10.1, respectively. On the other hand, if the solvent is poor ($u < 0$), then the buildup of segment density due to monomer–monomer interactions and the attractive surface–polymer interactions reinforce each other so that the attractive ΔF becomes steeper and shorter ranged.

5. Conclusions

Considering a planar surface with many terminally attached chains at a give distance from another similar surface (type b) or simply a hard wall (type a), we have approximated the problem by a one-dimensional diffusion problem for the probability distribution function for a chain by using the self-consistent field method of Edwards.[34] This approximation is good if the surface coverage of the polymer is large enough. Therefore the following conclusions are valid only in the high surface coverage regime.

We have solved the diffusion equation numerically by employing a self-consistent iterative scheme for different values of the excluded volume parameter u and the Hamaker constant ϵ/l for the adsorption of a polymer segment. The major conclusions are the following.

(1) The excluded volume effect broadens the segment density profile. For $u < 0$, the density profile is sharply peaked. As the adsorption energy increases all the profiles become broader but eventually peak near the surfaces. In general, the density profiles broaden as the surfaces are moved further apart.

(2) For type a, where bridging is forbidden, and $\epsilon = 0$ (no adsorption to the surface), the free energy ΔF of separation is purely repulsive and is long-ranged for both $u > 0$ and $u < 0$. As u is decreased, the range of repulsion is reduced but the steepness increases.

(3) For type a and $\epsilon > 0$ (no bridging but one surface can adsorb), ΔF is repulsive that Θ temperature and temperatures above Θ but with reduced range and steepness in comparison with the case of $\epsilon = 0$. On the other hand, the $\Delta F(d)$ profile exhibits a shallow free energy minimum if the temperature is below Θ, the depth of the minimum increasing with ϵ. Adsorption is responsible for attractive free energy profile in type a.

(4) For type b and $\epsilon = 0$ (no bridging and no adsorption of monomer), $\Delta F(d)$ profiles are purely repulsive for the Θ temperature and temperatures above Θ. But $\Delta F(d)$ shows a shallow free energy minimum if the temperature is below Θ. These are in good agreement with the recent experimental observations.[31,32]

(5) For type b and $\epsilon > 0$ (bridging is allowed), $\Delta F(d)$ profiles exhibit attractive minima even for temperatures above Θ.

Acknowledgment. This work was supported by National Science Foundation Grant No. DMR-8420962 and the Materials Research Laboratory at the University of Massachusetts.

References and Notes

(1) Napper, D. H. *Polymeric Stabilization of Colloidal Dispersion*; Academic: New York.
(2) Hasselink, F. Th. *J. Phys. Chem.* **1969**, *73*, 3488.
(3) Di Marzio, E. A.; Rubin, R. J. *J. Chem. Phys.* **1971**, *55*, 4318.
(4) Dolan, A. K.; Edwards, S. F. *Proc. R. Soc. London, Ser. A* **1974**, *337*, 59.
(5) Dolan, A. K.; Edwards, S. F. *Proc. R. Soc. London, Ser. A* **1975**, *343*, 427.
(6) de Gennes, P.-G. *J. Phys. (Les Ulis, Ft.)* **1976**, *37*, 1443.
(7) Alexander, S. *J. Phys. (Les Ulis, Fr.)* **1977**, *38*, 983.
(8) Levine, S.; Thomlinson, M. M.; Robinson, K. *Faraday Discuss.* **1978**, *65*, 202.
(9) Scheutjens, J. M. H. M.; Fleer, G. J. *J. Phys. Chem.* **1979**, *83*, 1619; **1980**, *84*, 173.
(10) de Gennes, P.-G. *Macromolecules* **1980**, *13*, 1069.

(11) Cosgrove, T. *Macromolecules* **1982**, *15*, 1290.
(12) Klein, J.; Pincus, P. *Macromolecules* **1982**, *15*, 1129.
(13) Croxton, C. *J. Phys. A* **1983**, *16*, 4343.
(14) Ben-Shaul, A.; Szleifer, I.; Gelbart, W. M. *J. Chem. Phys.* **1985**, *83*, 3597.
(15) Scheutjens, J. M. H. M.; Fleer, G. J. *Macromolecules* **1985**, *18*, 1882.
(16) Cosgrove, T.; Heath, T.; van Lent, B.; Leermakers, F.; Scheutjens, J. *Macromolecules* **1987**, *20*, 1692.
(17) Cosgrove, T.; Cohen Stuart, M. A.; Vincent, B. *Adv. Colloid Interface Sci.* **1986**, *24*, 143.
(18) Helfand, E.; Wasserman, Z. R. *Macromolecules* **1978**, *11*, 960.
(19) Noolandi, J.; Hong, K. M. *Macromolecules* **1982**, *15*, 482.
(20) Gerber, P. R.; Moore, M. A. *Macromolecules* **1977**, *20*, 476.
(21) Semenov, A. N. *Sov. Phys.-JETP (Engl. Transl.)* **1985**, *61*, 733.
(22) Milner, S. T.; Witten, T. A.; Cates, M. E., preprint.
(23) Takahashi, A.; Kawaguchi, M. *Adv. Polym. Sci.* **1982**, *46*, 1.
(24) Israelachvili, J. N.; Adams, G. E. *Nature (London)* **1976**, *262*, 774.
(25) Israelachvili, J. N.; Adams, G. E. *J. Chem. Soc., Faraday Trans. 1* **1978**, *74*, 975.
(26) Klein, J. *Nature (London)* **1980**, *288*, 248.
(27) Klein, J. *J. Chem. Soc., Faraday Trans. 1* **1983**, *79*, 99.
(28) Israelachvili, J. N.; Tirrell, M.; Klein, J.; Almog, Y. *Macromolecules* **1984**, *17*, 204.
(29) Klein, J.; Luckham, P. F. *Macromolecules* **1984**, *17*, 1041.
(30) Almog, Y.; Klein, J. *J. Colloid Interface Sci.* **1985**, *106*, 33.
(31) Hadziioannou, G.; Patel, S.; Granick, S.; Tirrell, M. *J. Am. Chem. Soc.* **1986**, *108*, 2869.
(32) Taunton, H. J.; Toprakcioglu, C.; Fetters, L. J.; Klein, J. *Nature (London)* **1988**, *332*, 712.
(33) Yamakawa, H. *Modern Theory of Polymer Solutions*; Harper and Row: New York, 1971.
(34) Edwards, S. F. *Proc. Phys. Soc., London* **1965**, *93*, 605.
(35) Ho, J.-S.; Muthukumar, M., submitted for publication in *Macromolecules*.
(36) Cosgrove, T.; Heeth, T. G.; Ryan, K.; Crowley, T. L. *Macromolecules* **1987**, *20*, 2879.

Dielectric Dispersion of Narrow-Distribution Poly(hexyl isocyanate) in Dilute Solution

Sanaye Takada, Takashi Itou, Hideaki Chikiri, Yoshiyuki Einaga, and Akio Teramoto*

Department of Macromolecular Science, Osaka University, Toyonaka, Osaka, 560 Japan.
Received May 25, 1988; Revised Manuscript Received July 20, 1988

ABSTRACT: Dielectric dispersion measurements were made on dilute solutions of narrow-distribution poly(hexyl isocyanate) in toluene to obtain the mean-square dipole moment $\langle\mu^2\rangle$ and dielectric relaxation time τ_D as functions of molecular weight and temperature. Analysis of the data for $\langle\mu^2\rangle$ at 25 °C in terms of the wormlike chain model of Kratky and Porod yielded a value of 27 700 for qM_L, with q and M_L being the persistence length and molar mass per unit contour length of the polymer, respectively. The data for τ_D at 25 °C as a function of molecular weight were accurately described by the equation for τ_D of Yoshizaki and Yamakawa for wormlike cylinders, and the result of the analysis was combined with the above qM_L value to give M_L = 740 nm^{-1}, q = 37 nm, and d = 1.5 nm, with d being the diameter of the cylinder. These parameter values were in good agreement with those estimated previously from viscosity data. The τ_D data at 10 and 40 °C were also represented by the same equation with the parameter values determined from viscosity data at the respective temperatures, thus establishing the validity of the Yoshizaki–Yamakawa theory of τ_D. The measured dielectric dispersions corrected for the sample's polydispersity in molecular weight were still polydisperse with respect to relaxation time, and the polydispersity increase with increasing molecular weight was more remarkable than predicted by the Yoshizaki–Yamakawa theory.

From various solution properties,[1-8] polyisocyanates of the general repeating unit –NRCO– are shown to be semiflexible; that is, they belong to those polymers classified between rodlike polymers and flexible polymers. Their conformational characteristics such as the mean-square radius of gyration etc. are well described by the wormlike chain model of Kratky and Porod.[1,4,6-8] Due to large cumulative dipole moments along their backbone chains, they exhibit dilute solution dielectric dispersions depending remarkably on molecular weight.[1-4,9,10] It is also noted that the reported dielectric dispersions in dilute solution cannot be described by the dispersion of the Debye type; in other words, they are usually polydisperse in relaxation time.[1,2,9,10] The reason for this polydispersity, among others, may be the sample's polydispersity in molecular weight and the presence of internal motional modes. In this connection, Yoshizaki and Yamakawa[11] have recently developed a theory of dielectric dispersion of helical wormlike chains in dilute solution, which gives an expression of the dielectric relaxation time τ_D and predicts a dielectric dispersion polydisperse with respect to relaxation time. They have treated the wormlike chain of Kratky and Porod as a special case of helical wormlike chains.

In the present study, we measured the dielectric constant and loss of dilute solutions of poly(hexyl isocyante) (PHIC) in toluene using narrow-distribution samples covering a range of molecular weight between 4410 and 910000. We have chosen this polymer because, in addition to the fact that it has been studied extensively with respect to the wormlike chain nature,[1,4,6-8] it is shown to have varying stiffness depending on the solvent conditions employed.[5-8,12] Thus the purpose of the present study is to provide dielectric dispersion data for PHIC free from molecular weight polydispersity and information about the polydispersity in dielectric relaxation time, thus enabling one to examine the quantitative validity of the theoretical predictions.

Experimental Section

Poly(hexyl isocyanate) samples were synthesized by polymerizing hexyl isocyanate in a toluene–dimethylformamide mixture with NaCN dispersed in dimethylformamide as an initiator.[13,14] Thirteen samples thus synthesized weighing about 130 g were separated into a number of fractions and 16 middle fractions were chosen for the present study. Their molecular weights and molecular weight distributions were determined by light scattering, sedimentation equilibrium, and gel permeation chromatography (GPC) as described elsewhere.[8] The numerical results are sum-

0024-9297/89/2222-0973$01.50/0